Spectrum of Engineering Sciences
ISSN (e) 3007-3138 (p) 3007-312X Volume 3, Issue 10, 2025

THERMODYNAMIC ANALYSIS OF COMBINED COOLING, WATER, AND POWER PLANT INTEGRATED WITH PARABOLIC TROUGH SOLAR COLLECTORS AND THERMAL ENERGY STORAGE SYSTEM

MOHAMMAD AADIL[*1], TEEKAM DAS[2], JAMSHED AALAM KALHAR[3]

[*1,2,3]*Department of Mechanical Engineering, Mehran University of Engineering and Technology, Jamshoro, Pakistan*

[*1]aadil124bhutto@gmail.com

DOI: https://doi.org/10.5281/zenodo.17278143

Keywords
Polygeneration
Parabolic Trough Solar Collectors
Desalination
Organic Rankine Cycle
Energy and Exergy Analysis
Renewable Energy
Vapor Absorption Refrigeration Cycle

Article History
Received: 01 July 2025
Accepted: 25 September 2025
Published: 06 October 2025

Corresponding Author: * Mohammad Aadil

Abstract

This study presents a detailed thermodynamic analysis of a solar-powered poly-generation system employing parabolic trough collectors. The system integrates an organic Rankine cycle (ORC) for power generation, a multiple-effect distillation (MED) unit for desalination, and a Vapor Absorption Refrigeration Cycle (VARC) for cooling. The analysis is performed by solving the mass, energy, and exergy balance equations for all system components, utilizing technical specifications of the subsystems and the thermodynamic properties of the working fluids. A computer model was developed and validated for this purpose. The performance of the poly-generation plant was evaluated under the climatic conditions of Lahore, Pakistan, across a range of operating parameters. System performance was assessed using multiple indicators: the Energy Utilization Factor (EUF), Artificial Thermal Efficiency (ATE), Fuel Energy Saving Ratio (FESR), and Exergy Efficiency. The primary results indicate that the EUF, ATE, and FESR trends correlate strongly with solar irradiance, peaking at midday. In contrast, the exergy efficiency was lowest at midday due to increased irreversibility from high temperatures. The EUF consistently recorded the highest values among the metrics. All performance parameters demonstrated higher values during the summer compared to the winter. The maximum instantaneous outputs for the winter day were 506 kW, 1061 kW, and 1628 kW for power, cooling, and desalination heat, respectively, which were surpassed by the summer day outputs of 558 kW, 1350 kW, and 2063 kW. Furthermore, freshwater production reached peaks of 6 kg/s in winter and 7.6 kg/s in summer.

INTRODUCTION

Global energy demand has experienced a substantial increase, a trend extensively documented and attributed to persistent population growth, accelerated urbanization, improved living standards, and industrial and economic development [1,2]. Fossil fuels, namely coal, crude oil, and natural gas, have historically constituted the primary energy supply, accounting for over 85% of global consumption [3]. The dependency on these resources has subsequently induced significant instability in energy markets and driven a surge in energy costs [4]. These challenges are further exacerbated by the detrimental environmental impact of fossil fuel combustion [5], most notably its contribution to

climate change and global warming [6]. Therefore, the development of renewable, clean, and carbon-neutral energy alternatives for power generation is imperative. This transition is essential to mitigate these adverse environmental effects and facilitate the production of sustainable electricity.

Solar energy is a key sustainable solution to contemporary challenges such as fossil fuel depletion, climate change, and growing energy demand. It is among the most prevalent and promising renewable resources [7], distinguished by its abundance, accessibility, favorable economics, and lack of harmful atmospheric emissions [8]. The application of solar energy in polygeneration systems, which are defined as energy systems producing three or more useful outputs like combined cooling, heating, and power (CCHP), represents an efficient method for generating multiple energy services from a single clean source [9,10]. Flat plate collector, evacuated tubes, parabolic trough collector, linear Fresnel reflector, solar dish concentrator, solar tower and thermal photovoltaics are the main technologies which are used to harness the solar energy for multiple purposes. Of the available solar technologies, the parabolic trough collector (PTC) is the most established and has been deployed commercially for decades [11,12]. This system employs a linear parabolic mirror to focus beam solar radiation on an evacuated tube receiver, typically operating at temperatures up to 400-500 °C using heat transfer fluids like thermal oils or molten salts. Commonly featuring a single-axis tracking system, PTCs are applicable in power generation, industrial heat, cooling, and polygeneration systems. Properly configured cogeneration and trigeneration systems demonstrate proven capabilities for the simultaneous production of different energy services. These systems achieve higher exergy efficiency, lower economic costs, and reduced pollutant emissions through effective process integration [13].

A substantial body of research has emerged focused on generating multiple useful outputs through various system configurations of renewable energy sources. For example, Temiz and Dincer [14] developed a system utilizing both solar and geothermal energy to co-produce hydrogen, freshwater, electricity, and heat. In their design, solar energy collected by parabolic trough solar collectors heats a molten salt working fluid. This high-temperature fluid subsequently provides heat for a thermochemical process to generate hydrogen. The geothermal energy component is used both to power a desalination unit for seawater and to drive a Rankine cycle for electricity generation. The reported energy and exergy efficiencies for this system were 27.4% and 17.3%, respectively. Serra et al. [15] explored the fundamental concepts of polygeneration and energy integration, illustrating them with practical applications. These examples included a sugarcane processing plant co-producing sugar and energy, a district heating and cooling system powered by natural gas cogeneration engines, and a combined facility for water and energy production. Yuksel and Ozturk [16] developed an integrated system based on solar and biomass energy for the generation of power, hot water, heating, and cooling. In their configuration, solar energy collected by a parabolic trough collector was used to drive a Rankine cycle, while biomass combustion provided a supplementary renewable heat source. They reported maximum energy and exergy efficiencies for the system of 59.16% and 54.23%, respectively.

In a separate techno-economic analysis, Nixon et al. [17] evaluated the feasibility of hybrid solar-biomass power plants for polygeneration applications, including electricity and process heat production. Their assessment considered plants with peak thermal capacities ranging from 2 MW to 10 MW, using technical, financial, and environmental criteria. Loni et al. [18] conducted an experimental investigation of a solar-driven organic Rankine cycle (ORC) system. In their empirical study, the solar receiver and condenser inlet temperatures were maintained at 50°C and 37°C, respectively, using R601 as the ORC working fluid. Their results indicated that the maximum exergy efficiency was achieved at a turbine inlet pressure of 20 bar. Atiz et al. [19] developed a hybrid system that integrates solar and geothermal energy to power an organic Rankine cycle (ORC) for electricity generation, evaluating its performance across a solar irradiation range of 200 to 1000 W/m². The study investigated three different ORC working fluids: n-hexane, n-pentane, and n-butane. The results indicated that the system's overall efficiency is a function of both the geothermal resource temperature and the selected working fluid. The maximum reported energy and exergy efficiencies were 6.92% and 21.06%, respectively. Al-Sulaiman et al. [20]

conducted energy and exergy analyses of a biomass fueled trigeneration system incorporating an organic Rankine cycle (ORC). The study evaluated four operational modes: electricity generation only, combined power and cooling, combined power and heating, and full trigeneration. The analysis considered parameters such as the ORC evaporator pinch point temperature, and the pump inlet temperature and pressure. The results identified the biomass burner and the ORC evaporator as the primary sources of exergy destruction, contributing 55% and 38% of the total, respectively. In a separate study, Maraver et al. [21] assessed a polygeneration system for simultaneous energy and water production. The system utilized an ORC for combined heat and power, coupled with multi effect distillation (MED) for desalination and cooling. The energy feasibility was evaluated using the fuel energy saving ratio (FESR). The analysis determined that the highest energy savings were achieved when heat was prioritized for domestic hot water production, which consequently limited the thermal energy available to activate the MED and other thermally driven subsystems. The ORC subsystem was modeled with several working fluids, leading to the conclusion that fluorobenzene and octamethyltrisiloxane were the most suitable candidates for the proposed polygeneration application.

Parabolic trough collectors (PTCs) are frequently employed in polygeneration systems due to their capacity to operate at elevated temperatures, typically up to 400–500 °C. This wide operational range enables their integration with numerous thermodynamic cycles and processes. A common configuration involves hybridizing PTCs with biomass boilers to ensure a continuous thermal energy supply, particularly during periods without solar irradiation. The thermal output is often utilized to drive absorption chillers for cooling production or to provide direct heating. The prime movers integrated with these systems typically include steam Rankine cycles, organic Rankine cycles (ORCs), internal combustion engines, and gas turbines. A summary of representative studies on PTC-based polygeneration systems is provided in Table 1.

Table 1

Study	Useful outputs	Prime mover	Conclusions
Mathkor et al. [22]	Cooling, Electricity, Fresh water	ORC	η_{ex} = 41.7%
Ezzat and Dincer [23]	Refrigeration, Industrial heat, (DHW), Drying, Electricity	Rankine water/steam	η_{en} = 69.8% η_{ex} = 42.8%
Chadegani et al. [24]	Heating, Cooling, Electricity, Hydrogen, Fresh water	ORC (double)	η_{en} = 33.5% η_{ex} = 20.7%
Ozlu and Dincer [25]	Heating, Fresh water, Electricity, Hydrogen	Rankine water/steam	η_{en} = 36% η_{ex} = 44%
Al-Sulaiman et al. [26]	Heating, Cooling, Electricity	ORC	η_{ex} = 20%
Ozlu and Dincer [27]	Heating, Cooling, Electricity, Hydrogen	Kalina cycle	η_{en} = 57% η_{ex} = 36%
Bellos and Tzivanidis [28]	Heating, Cooling, Electricity	ORC	η_{en} = 152% η_{ex} = 29.4%
Li et al. [29]	Heating, Cooling, Electricity	Piston engine	η_{en} = 50.0%

Study	Useful outputs	Prime mover	Conclusions
Elsavi et al. [30]	Heating, Cooling, Electricity	ORC	η_{en} = 96% η_{ex} = 12.8%
El-Emam and Dincer [31]	Heating, Cooling, Electricity, Hydrogen, Fresh water	ORC	η_{ex} = 39%
Suleman et al. [32]	Heating, Cooling, Electricity, Drying	ORC (double)	η_{en} = 54.7% η_{ex} = 76.4%
Yang et al. [33]	Heating, Cooling, Electricity	Gas turbine (double)	PP = 6.07 years
Islam et al. [34]	Heating, Cooling, Electricity, Hydrogen, Oxygen	ORC (double)	η_{en} = 80% η_{ex} = 40%
Khalid et al. [35]	Heating, Cooling, Electricity	ORC	η_{en} = 46.1% η_{ex} = 7.3%
Calise et al. [36]	Heating, Cooling, Electricity, Fresh water	ORC	η_{ex} = 50%
Almahdi et al. [37]	Heating, Cooling, Electricity, Hydrogen, Dry sawdust biomass	ORC (double)	η_{en} = 20.7% η_{ex} = 13.7%
Yuksel et al. [38]	Heating, Cooling, Electricity, Hydrogen	ORC (double)	η_{en} = 16% η_{ex} = 8%
Bellos et al. [39]	Heating (two temperature levels, Cooling, Electricity	ORC	η_{en} = 51.3% η_{ex} = 21.8% PP = 5.13 years
Karellas et al. [40]	Heating, Cooling, Electricity	ORC	η_{ex} = 7% PP = 7 years
Al-Ali and Dincer [41]	Heating (building-industrial), Cooling, Electricity	ORC (triple)	η_{en} = 78.0% η_{ex} = 36.6%
Pantaleo et al. [42]	Heating, Cooling, Electricity	Gas turbine	NPV = 13 k€ IRR = 30%
Wu et al. [43]	Heating, Cooling, Electricity	ORC	30% cost reduction
Dabwan et al. [44]	Electricity, Cooling, Fresh water	Gas turbine	30% lower CO_2 emissions
Khalid et al. [45]	Heating, Cooling, Electricity	Gas turbine	η_{en} = 91.0% η_{ex} = 34.9%
Li et al. [46]	Heating, Cooling, Electricity	Piston engine	η_{en} = 50.0%

Study	Useful outputs	Prime mover	Conclusions
Li et al. [47]	Heating, Cooling, Electricity	Piston engine	η_{ex} = 19.2%
Calise [48]	Heating, Cooling, Electricity	Fuel cell	η_{ex} = 44.7% SF = 87% SPP = 3.3 years
Wang et al. [49]	Heating, Cooling, Electricity, Methanol	Fuel cell	η_{en} = 73.7%/51.7% η_{ex} = 18.8%/26.1% (summer/winter)
Bellos and Tzivanidis [50]	Heating, Cooling, Electricity	Modified ORC	η_{en} = 87.4% η_{ex} = 11.3% SPP = 3 years
Elsavi et al. [51]	Heating, Cooling, Electricity	ORC	η_{en} = 96% η_{ex} = 12.8%

The theoretical framework of exergy and its critical relationship with environmental impact, sustainability, and energy management has been extensively examined in the literature [52, 53]. Furthermore, numerous researchers have demonstrated the importance of exergy analysis for the evaluation of combined heat and power (CHP) and trigeneration systems [54]. For instance, Minciuc et al. [55] introduced a methodological approach for analyzing trigeneration systems and establishing the thermodynamic performance limits for gas turbine-based systems with absorption chilling. In a related study, Ahmadi et al. [56] performed an exergo-environmental analysis of an integrated organic Rankine cycle for trigeneration. Their results indicated that the trigeneration system achieves a higher exergy efficiency compared to conventional CHP systems or standalone gas turbine cycles, while also resulting in lower carbon dioxide emissions. The performance assessment of polygeneration systems employs various criteria and definitions. Commonly used metrics include energy-based efficiencies, such as the utilization factor, which assign equal value to power and heat outputs without accounting for their differing energy qualities. In contrast, exergy analysis, which incorporates both the first and second laws of thermodynamics, provides a performance evaluation from both quantitative and qualitative perspectives. Minciuc et al. [55] noted that because the cooling subsystem in a polygeneration system can employ a refrigeration machine with a coefficient of performance (COP) greater than unity, the calculated system efficiency can also exceed 100% when based solely on energy. This has prompted discussions on appropriate performance definitions, with the fuel energy saving ratio emerging as a reliable thermodynamic performance criterion for cogeneration and polygeneration systems in several studies [57, 58]. The co-production of fresh water in dual or multi-purpose plants is recognized as a more reliable and efficient approach compared to standalone desalination facilities. El Nashar [59] provided a comprehensive review of cogeneration for power and desalination, outlining a methodology for selecting the optimal configuration based on specific water and power demands.

This study aims to conduct a thermodynamic analysis of a solar-driven poly-generation system that utilizes an Organic Rankine Cycle (ORC) as its prime mover. The analysis involves modeling and assessing the system's performance by evaluating the variable energy production rates for electricity, desalination, and cooling. These rates are determined for representative summer and winter days under the climatic conditions of Lahore, Pakistan. The system's overall performance is further evaluated using a set of key performance indicators derived from both energy and exergy principles.

2. Methods

A comprehensive description of the proposed system is provided in the System Description section. Each subsystem was subjected to a detailed thermodynamic analysis to derive the governing energy and exergy efficiency equations. The mass, energy, entropy, and exergy balance equations, as presented in the tables within that section, were applied to compute the unknown thermodynamic properties at each state point and the corresponding capacities of all inputs and outputs.

2.1 **System Description**

The poly-generation system under investigation integrates four primary subsystems: a parabolic trough solar collector (PTSC) field, an organic Rankine cycle (ORC) for power generation, a multi-effect distillation (MED) unit for freshwater production, and a single-effect absorption chiller for cooling. The simultaneous output of electrical power, potable water, and cooling is illustrated in the system schematic (Fig. 1).

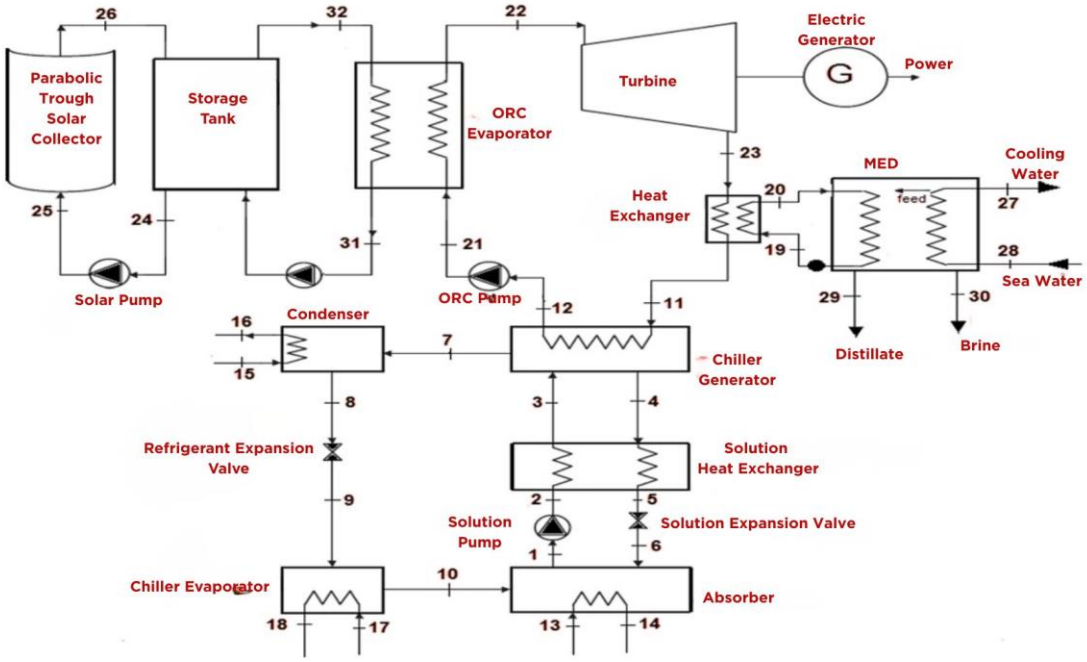

Figure 1

The selection of an appropriate working fluid is a critical determinant of ORC performance. Key selection criteria include a high critical temperature to enable efficient utilization of the available thermal energy, alongside considerations of cycle efficiency, requisite equipment size, and environmental impact [60, 61]. For this analysis, O-xylene was selected as the ORC working fluid. This selection is justified by its high critical temperature (630 K), which is well-suited to the operating temperature range of the PTSC field, and its associated high cycle efficiency. The solar energy collection subsystem comprises a field of parabolic trough collector modules, each with a length of 14 m [62]. The system employs Therminol VP-1 as the heat transfer fluid (HTF), circulated through a receiver pipe encapsulated within a vacuum annulus to minimize convective and radiative heat losses (detailed specifications are provided in Table 2). Therminol VP-1 was chosen for its exceptional thermal stability and favorable thermophysical properties, including low viscosity, which promotes efficient heat transfer across a broad operational temperature range of 12–400°C [63]. Its proven reliability in numerous commercial PTSC-based power plants further validates its selection [64].

Table 2

Parameters	Value

Isentropic turbine efficiency, %	85
Isentropic pump efficiency, %	80
Motor efficiency, %	95
Generator efficiency, %	90
Turbine inlet pressure, MPa	2
Pump inlet temperature, °C	90
Aperture width, m	6
PTC Length per module, m	12
Receiver Inner diameter, m	0.09
Receiver Outer diameter, m	0.0787
Glass cover diameter, m	0.120
Transmissivity of the receiver	0.79
Absorptivity of the receiver	0.80
Reflectivity of the aperture surface	0.98
Intercept angle	1
Receiver emittance	0.96
Glass cover emittance	0.90
Mass flow rate of heat transfer fluid, kg s–1	3.89
Solution heat exchanger effectiveness	0.65
Solution pump mass flow rate, kg/s	1.8
Cooling water mass flow rate to absorber, kg/s	11.87
Cooling water inlet temperature, °C	25
Overall heat conductance of generator, kW/K	1.89
Overall heat conductance of condenser, kW/K	1.6
Overall heat conductance of evaporator, kW/K	1.4
Overall heat conductance of absorber, kW/K	2.34

The integration of a Thermal Energy Storage (TES) system is critical for mitigating the inherent intermittency of solar radiation and ensuring stable, continuous operation of the poly-generation plant. The system employs a single-tank thermocline configuration, a design that offers a balance between performance and cost-effectiveness compared to dual-tank systems. In this design, a single, vertically oriented tank contains the storage medium. A thermally stable solid filler material, typically quartzite rock or ceramic bed, is packed within the tank and serves as the primary thermal mass. The interstitial spaces within this packed bed are filled with the heat transfer fluid (HTF), Therminol VP-1. This arrangement creates a thermal gradient, or "thermocline," a distinct horizontal layer that separates the high-temperature fluid at the top from the low-temperature fluid at the bottom.

The operational strategy is bifurcated into two primary modes:

Charging Mode: During periods of high solar insolation, surplus thermal energy is used to charge the TES. Hot HTF from the solar collector field is introduced at the top of the storage tank. As it percolates downward through the packed bed, it transfers heat to the solid filler material. The cooler HTF, displaced from the bottom of the tank, is returned to the solar field for reheating. This process steadily pushes the thermocline layer downward, increasing the volume of high-temperature storage medium.

Discharging Mode: When solar irradiance is insufficient, the system discharges the stored thermal energy. The flow direction is reversed: cool HTF from the ORC loop is pumped into the bottom of the tank. As this fluid moves upward, it is heated by the hot solid filler material. The now-hot HTF exits from the top of the tank and is directed to the ORC evaporator

to drive the cycle. This process moves the thermocline layer upward until the stored energy is depleted.

The primary advantage of the single-tank thermocline system is a significant reduction in capital cost, as it eliminates the need for a second storage tank and reduces the total volume of often-expensive HTF required. The use of a low-cost solid filler material provides the majority of the thermal capacity. A key technical challenge is maintaining the stability and sharpness of the thermocline zone to prevent thermal mixing, which is mitigated through careful tank design and flow management. This integrated TES subsystem is essential for transforming the poly-generation plant from a solar-following unit into a more dispatchable and reliable energy asset.

2.2 Analysis of the poly-generation system

The thermodynamic model of the poly-generation system is developed based on fundamental principles of energy and exergy analysis. The governing equations derived from these analyses were programmed and solved computationally using the Engineering Equation Solver (EES) software [65]. To facilitate theoretical analysis, the following assumptions were adopted:

General System Conditions:

- The system operates under a quasi-steady state condition.
- Pressure drops and heat losses across all pipelines and heat exchangers are neglected.
- Changes in kinetic and potential energy, as well as the corresponding exergy components, are considered negligible.
- The chemical exergy of all material streams is neglected, with the exception of the saline water analyzed within the Multi-Effect Distillation (MED) subsystem.
- The reference environment (dead state) for exergy analysis is defined by a temperature (T_0) of 25°C, a pressure (P_0) of 101.325 kPa, and a seawater salinity (X_0) of 42 g/kg, representative of the Arabian Gulf.

Organic Rankine Cycle (ORC) Assumptions:

- The working fluid at the ORC pump inlet is in a saturated liquid state.

Absorption Chiller Assumptions:

- The refrigerant at the outlet of the condenser is saturated liquid, and at the outlet of the evaporator is saturated vapor.
- The pump work input for the absorption cycle is neglected due to its insignificance relative to the thermal energy input required by the generator.

Multi-Effect Distillation (MED) Assumptions:

- The steam supplied to the MED unit is saturated.
- The temperature difference between the feed water and the cooling water is maintained at 10°C.
- The temperature difference between the boiling brine in the last effect and the feed water is maintained at 5°C.

2.2.1 Energy Analysis

2.2.1.1 Solar energy collecting system

The modeling of the parabolic trough collector (PTC) subsystem is based on established methodologies found in the literature [66, 67]. The model equation for each quantity is defined in Table 3.

Table 3

Rate of Useful Energy Delivered From a PTC	$Q_u = A_{ap}F_R(S - \frac{A_r}{A_{ap}}U_L(T_{fi} - T_a))$	F_R is the heat removal factor, S is the heat absorbed by the receiver, A_{ap} is the aperture area, A_r is the receiver area, and U_L is the solar collector overall heat loss coefficient.
Heat Absorbed by the Receiver	$S = G_b\eta_r$	G_b is the direct irradiation intensity and η_r is receiver efficiency.

Receiver Efficiency	$\eta_r = \rho\gamma\tau\alpha K$	ρ, γ, τ, α and K are the reflectance of the mirror, intercept factor, transmittance of the glass cover, absorptance of the receiver and incidence angle modifier respectively.
Heat Removal Factor	$F_R = \frac{m_r C_{pr}}{A_r U_L}\left[1-\exp\left(-\frac{A_r U_L F_l}{m_r C_{pr}}\right)\right]$	m_r is mass flow rate through the receiver, C_{pr} is the specific heat of heat transfer fluid inside the receiver and F_l is the collector efficiency factor.
Collector Efficiency Factor	$F_l = \frac{1/U_L}{\frac{1}{U_L}+\frac{D_o}{D_i h_{fi}}+\frac{D_o}{2k}\ln\left(\frac{D_o}{D_i}\right)}$	k is the thermal conductivity of the receiver tube and h_{fi} is the convection heat transfer coefficient inside the receiver tube
Solar Collector Heat Loss Coefficient between Ambient and Receiver	$U_L = \left[\frac{A_r}{(h_{c,ca}+h_{r,ca})A_c}+\frac{1}{h_{r,cr}}\right]^{-1}$	N/A
Radiation Heat Coefficient between the Ambient and the Cover	$h_{r,ca} = \varepsilon_c\sigma\left(T_c+T_a\right)\left(T_c^2+T_a^2\right)$	σ is Stefan–Boltzmann constant and E_c is the emittance of the cover.
Radiation Heat Transfer Coefficient between the Cover and the Receiver	$h_{r,cr} = \sigma\frac{(T_c+T_r)(T_c^2+T_r^2)}{1/\varepsilon_r+(A_r/A_c)(1/\varepsilon_c-1)}$	T_r is the receiver's average temperature.
Cover Temperature of the Receiver	$T_c = \frac{A_r h_{r,cr} T_r + A_c(h_{c,ca}+h_{r,ca})T_a}{A_r h_{r,cr}+A_c(h_{c,ca}+h_{r,ca})}$	N/A
Total Energy Input to the System	$\dot{Q}_{solar} = A_{ap}\,F_R\,S\,N_t$	N_t is the total number of collectors and A_{ap} is the aperture area.
Aperture Area	$A_{ap} = (w-D_{co})L$	L, w, and D_{co} are the collector (module) length, width and receiver cover outer diameter respectively.
Thermal Energy Storage System Energy Balance	$\left[(mC_p)_s\right]dT_s/dt = Q_u - Q_{load} - (UA)_s.(T_s-T_a)$	m is the mass of fluid (Therminol VP-1) in the storage unit and C_p is the specific heat capacity of fluid (Therminol VP-1) in the storage. T_a is the ambient temperature around the tank. Q_u and Q_{load} represent the useful gain from the solar collector and the energy needed by the absorption system respectively. $(UA)_s$ is the

		liquid storage tank loss coefficient area product.

2.2.1.2 Organic Rankine cycle system

The organic Rankine cycle subsystem is modeled based on mass and energy conservation laws. The modelling equations are given in Table 4.

Table 4

Heat Addition into the Power cycle	$\dot{Q}_E = \dot{m}_f (h_{22} - h_{21})$	m_f is the mass flow rate of the organic working fluid.
Power Output of the Turbine	$\dot{W}_T = \dot{m}_f (h_{22} - h_{23})$	N/A
Isentropic Efficiency of the Turbine	$\eta_T = \frac{h_{22} - h_{23}}{h_{22} - h_{23s}}$	N/A
Isentropic Efficiency of the Pump	$\eta_p = \frac{h_{21s} - h_{12}}{h_{21} - h_{12}}$	N/A
Pump Power Input (ORC)	$\dot{W}p_{,ORC} = \dot{m}_f (h_{21} - h_{12})$	N/A
Pump Power Input (Solar)	$\dot{W}_{p,solar} = \dot{m}_t (h_{25} - h_{24})$	m_f is mass flow rate of heat transfer working fluid (Therminol VP-1)
Net Electrical Power Output	$\dot{W}_{net,el} = \dot{W}_T \eta_g - \dot{W}_{p,ORC} / \eta_{motor} - \dot{W}_{p,solar} / \eta_{motor}$	N/A

2.2.1.3 Vapor Absorption Refrigeration Cycle

The absorption chiller utilizes a lithium bromide-water (LiBr-H_2O) solution as its working fluid. The subsystem is modeled by applying the fundamental principles of mass and energy conservation to a control volume encompassing each major component: the generator, condenser, evaporator, absorber, and solution heat exchanger. The modelling equations are given in Table 5.

Table 5

Heat input to the Generator	$Q_{gen} = m_7 h_7 + m_4 h_4 - m_3 h_3$
Heat rejected from the Condenser	$Q_{cond} = m_7 h_7 - m_8 h_8$
Heat Removal from the Absorber	$Q_{abs} = m_{10} h_{10} + m_6 h_6 - m_1 h_1$
Heat added to the Evaporator	$Q_{chiller,evap} = m_{10} h_{10} - m_9 h_9$

Energy Balance on the hot side of Solution Heat Exchanger	$Q_{hx-h} = m_4h_4 - m_5h_5$
Energy Balance on the cold side of Solution Heat Exchanger	$Q_{hx-c} = m_3h_3 - m_2h_2$

2.2.1.4 Multiple-Effect Distillation (MED) system
The modelling equations are given in Table 6:

Table 6

Amount of Energy Supplied to Saturated Steam	$\dot{Q}_{MED} = m_{19}(h_{20} - h_{19})$
Overall Mass Balance around the Plant (assume no salt) (m is the mass flow rate, x is the salinity, and the sub scripts b, d, and f denote the rejected brine, distillate, and feed seawater respectively)	$m_f = m_b + m_d$ $m_f x_f = m_b x_b$
Thermal Performance of the System (PR) (m_d is the total mass of the distillate produced)	$PR = \frac{m_d}{m_s}$
Specific Cooling Water flow rate	$sM_{cw} = \frac{m_{cw}}{m_d}$

The multi-effect distillation (MED) unit is modeled using established design correlations that describe the relationship between key performance indicators and primary operating parameters. These indicators include thermal performance, specific heat transfer area, and specific cooling water flow rate, which are correlated with the top brine temperature and the number of effects. The employed correlations were originally derived from a comprehensive systematic analysis of a forward feed MED plant [68]. The validity of this modeling approach has been confirmed in subsequent work by Mistry et al. [69]. The present analysis uses a configuration of ten effects. This number is selected as it is representative of industrial scale MED plants and is commonly used in previous research. Studies by Kamali et al. [70] and Zhao et al. [71] on the influence of the number of effects, denoted as n, on the Gain Output Ratio (GOR) demonstrate that while GOR increases significantly at low values of n, the rate of improvement diminishes considerably within the range of eight to ten effects. This justifies the selection of ten effects for this study, as it represents a point of operational maturity with diminishing returns for additional units. It is noted that qualitatively similar results would be expected with a closely related number of effects, such as eight or nine. The thermodynamic properties of seawater throughout the MED system are calculated using the integrated seawater library within the Engineering Equation Solver (EES) software [65].

2.2.2 Exergy Analysis

Exergy analysis overcomes numerous limitations inherent in conventional energy analysis by identifying the causes, locations, and magnitudes of thermodynamic inefficiencies within a system. A central concept in this analysis is exergy destruction, which represents the potential work lost due to irreversibilities. The total exergy destruction for the entire solar driven system is the sum of the exergy losses occurring in each individual component. For a control volume operating at steady state, the exergy destruction rate for any system component is defined by the following equation:

where: $\dot{E}x_{dest}$ is the exergy destruction rate (kW), $\dot{m}_i e_i$ and $\dot{m}_e e_e$ are the exergy flow rates (kW) at the inlets and outlets, respectively, $\dot{Q}_k$ is the heat transfer rate (kW) at a boundary where the temperature is T_k (K), $\dot{W}$ is the work transfer rate (kW), T_0 is the reference environmental temperature (K). The first two terms on the right-hand side, represent the net exergy transfer due to mass flow. The third term quantifies the exergy transfer associated with heat. The final term, $\dot{W}$, accounts for the exergy transfer due to work. For the absorption chiller subsystem, which employs a lithium bromide-water (LiBr-H_2O) solution as the working fluid, the calculation of exergy must include the chemical exergy component, requiring consideration of the solution concentration.

$$\psi = [h(T,X) - h_o] - T_o[s(T,X) - s_o]$$

The total exergy input to the solar-powered poly-generation system is defined as the exergy of

$$\dot{E}x_{in} = A_c G_b \left(1 + \frac{1}{3}\left(\frac{T_{amb}}{T_s}\right)^4 - \frac{4}{3}\left(\frac{T_{amb}}{T_s}\right)\right)$$

the solar radiation incident upon the collector aperture. This exergetic content is calculated as a function of the sun's effective outer surface temperature, which is taken to be 6000 K, in accordance with established practice for such analyses. It is calculated as:

2.2.3 System performance analysis

This section details the thermodynamic performance indicators employed to evaluate the cogeneration and

$$\dot{E}_{xd} = \sum_{in} \dot{m}\psi - \sum_{out} \dot{m}\psi + \sum\left(1 - \frac{T_o}{T_k}\right)\dot{Q}_k - \dot{W}$$

poly-generation system depicted in Figure 1. To quantitatively assess the advantages of multi-generation systems over conventional single-output plants, several established criteria are utilized. These include the Energy Utilization Factor (EUF), Primary Energy Savings (PES), Artificial Thermal Efficiency (ATE), Fuel Energy Saving Ratio (FESR), and Exergy Efficiency (ExEff). Each indicator provides a distinct perspective on system performance by focusing on different aspects of the energy flows, and their application can lead to varying interpretations. The EUF, ATE, and FESR are derived from the first law of thermodynamics, providing a quantitative assessment of energy conversion and utilization without accounting for energy quality. The Energy Utilization Factor measures the overall efficiency in converting input fuel into useful products. The Artificial Thermal Efficiency is applied when electricity generation is prioritized over thermal energy production, assigning it a higher weighting. The Fuel Energy Saving Ratio quantifies the reduction in primary energy consumption achieved by the poly-generation system compared to separate, conventional methods of producing the same outputs. In contrast, the Exergy Efficiency is grounded in the second law of thermodynamics. This metric evaluates the system's performance against an ideal, reversible benchmark, thereby providing a measure of thermodynamic perfection. The mathematical expressions for these performance criteria, as applied to the overall poly-generation system, are summarized in Table 7.

Table 7

EUF: Energy utilization factor	$EUF = \frac{\dot{W}_{net,el} + \dot{Q}_{evap} + \dot{Q}_{MED}}{\dot{Q}_{solar}}$
ATE: Artificial thermal efficiency	$ATE = \frac{\dot{W}_{net,el}}{\dot{Q}_{solar} - (\dot{Q}_{Evap} + Q_{MED}) / \eta_b}$
FESR: Fuel energy saving factor	$FESR = 1 - \frac{\dot{Q}_{Solar-Poly}}{(\dot{W}_{net,el} / \eta_{el}) + (\dot{Q}_{Evap} + Q_{MED}) / \eta_b}$

ExE_{ff} : Exergy efficiency	$\eta_{ex,poly} = \frac{\dot{W}_{net,ci} + m_{17}(\psi_{18} - \psi_{17}) + m_{19}(\psi_{20} - \psi_{19})}{\dot{E}x_{in}}$

2.2.4 Validation of the developed Model

2.2.4.1 Parabolic Trough Solar Collector Model

The solar collector model was validated by comparing its predictions with experimental data published by Kutscher et al. [72]. As illustrated in Figure 2, the comparison shows the variation

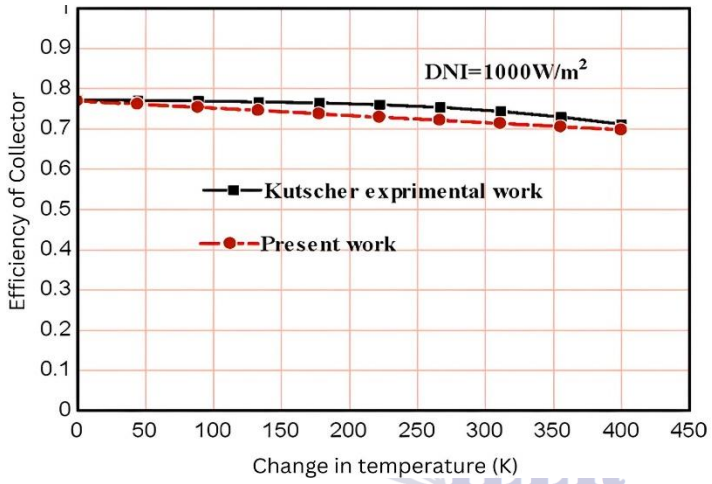

Figure 2

of collector efficiency with the temperature difference between the heat transfer fluid and the ambient air, under a direct normal solar irradiance of 1000 W/m². The results indicate general agreement between the simulated model and the experimental data. A slight deviation is observed, however, where the model's efficiency curve does not precisely match the experimental values across the entire temperature range, particularly at moderate temperature differences.

2.2.4.2 Oraganic Rankine Cycle Model

The validation of the Organic Rankine Cycle (ORC) model is presented in Figure 3. The figure compares the thermal efficiency of an ideal Rankine cycle using R-123 as the working fluid, as calculated by the present model, against the results reported by Hettiarachchi et al. [73]. The data

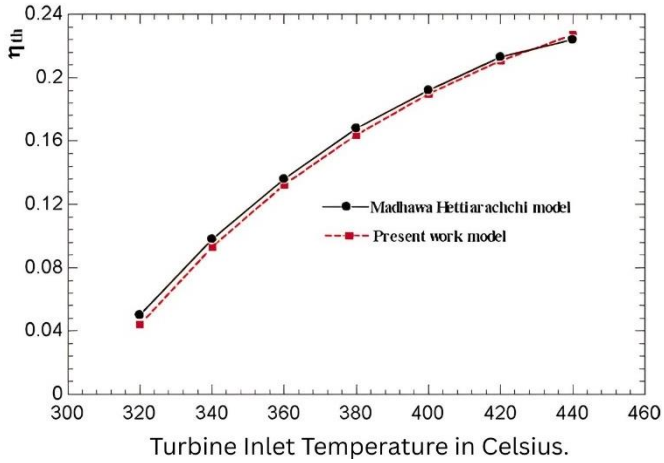

Figure 3

show close agreement between the results of this work and the reference data across the entire investigated range of turbine inlet temperatures.

2.2.4.3 Vapor Absorption Refrigeration Cycle

The model for the single-effect LiBr–H_2O absorption chiller was validated against the work of Balghouthi et al. [74], who evaluated the feasibility of solar-powered absorption cooling under

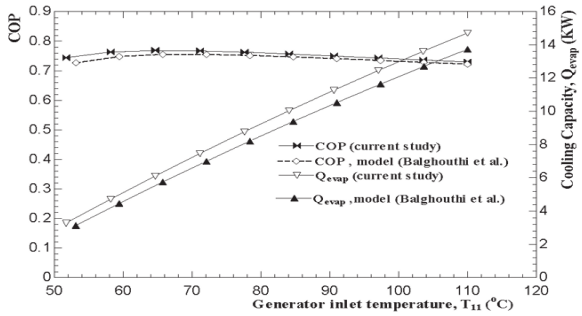

Figure 4

Tunisian climate conditions. In their study, a TRNSYS model was developed for an 11 kW single-effect absorption system designed for a 150 m^2 building. Figure 4 presents a comparison of the coefficient of performance and cooling load as functions of the generator inlet temperature. The results demonstrate close agreement between the present model and the simulation data from Balghouthi et al. [74].

3. Results and discussion

This section presents the findings from the energy and exergy analysis of the solar-driven poly-generation system. The energy analysis quantifies key output metrics, including the net electrical power generated by the Organic Rankine Cycle (ORC), the cooling capacity supplied by the absorption chiller, and the thermal energy required to produce saturated steam for the Multi-Effect Distillation (MED) unit. Subsequently, these results are synthesized to determine system-wide performance parameters, such as the Energy Utilization Factor (EUF) and Fuel Energy Saving Ratio (FESR). The discussion examines the dynamic performance of the system by analyzing the hourly variation of energy production rates (electricity, fresh water, cooling) over representative days. Furthermore, the daily evolution of key

performance indicators is evaluated to assess the system's thermodynamic and operational effectiveness under transient solar conditions. The interrelationship between operating parameters, such as solar irradiance and collector temperature, and the resulting energy and exergy efficiencies is investigated in detail.

It should be noted that the presented results were determined through a systematic exergy-based optimization procedure aimed at maximizing the overall exergy efficiency, or equivalently, minimizing the total exergy destruction within the system. For example, the turbine inlet pressure was identified as a key parameter and its value was established by evaluating the system's exergetic performance across a range of pressures. This optimization procedure determined that a turbine inlet pressure of 7 MPa yields the peak exergetic

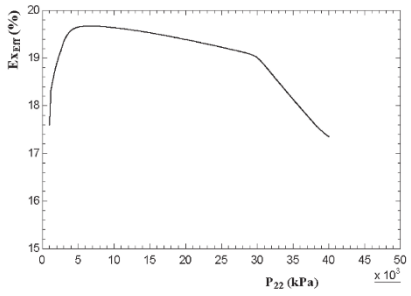

Figure 4

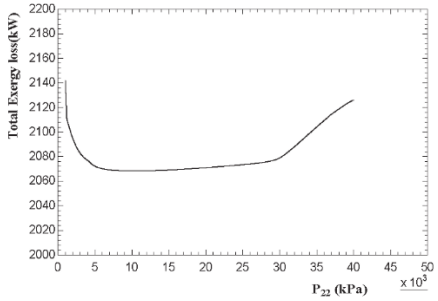

Figure 6

performance, corresponding to a maximum system exergy efficiency of 19.7% and a minimum total exergy destruction of 2068 kW, as illustrated in Figures 5 and 6, respectively. Consequently, this optimized value of 7 MPa was selected as the fixed turbine inlet pressure for all subsequent analysis in this study.

The simulation for this study is situated in Lahore, Pakistan (latitude: 31.5204° N, longitude: 74.3587° E), a location selected for its substantial solar energy potential. The system simulation utilizes measured meteorological data for representative summer and winter days, with the direct normal irradiance (DNI) and ambient temperature profiles serving as fundamental inputs, as shown in Figures 7 and 8, respectively. The solar radiation profile in Figure 7 demonstrates a characteristic pattern, with peak solar irradiance occurring at solar noon and diminishing during the early morning and late afternoon hours.

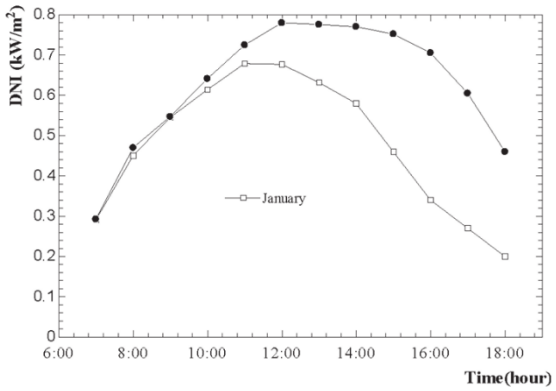

Figure 7

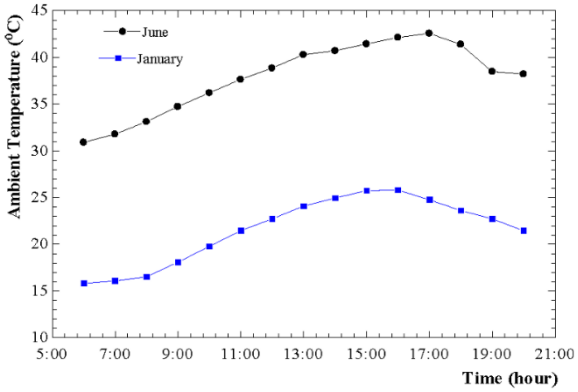

Figure 8

The performance of the poly generation system was evaluated using four key indicators: the Energy Utilization Factor (EUF), Artificial Thermal Efficiency (ATE), Fuel Energy Saving Ratio (FESR), and Exergy Efficiency (ExEff). Their hourly variations for representative summer and winter days are presented in Figures 9 and 10.

The EUF, ATE, and FESR exhibit a strong correlation with the direct normal irradiance profile shown in Figure 7. These parameters increase during the morning, reach their maximum values around solar noon, and decrease throughout the afternoon. In contrast, the exergy efficiency demonstrates an inverse pattern, with its highest values occurring during sunrise and sunset and its lowest point at midday. This counter trend is attributed to increased exergy destruction from greater thermodynamic irreversibilities when the temperature difference between the solar collection system and the environmental dead state is maximized. A comparison of the parameters shows that the EUF yields the highest numerical values, followed by the ATE. Furthermore, all performance indicators show consistently higher values during the summer day compared to the winter day, which reflects the greater solar resource availability and longer operational period in June.

Figures 11 and 12 present the temporal variation of the fresh water production rate and the power to water ratio for representative days in January and June. The fresh water production reaches maximum instantaneous values of 6 kg/s and 7.6 kg/s for the January and June days, respectively. These peak production rates occur at approximately 11:30 and 13:30 local time, corresponding with periods of high thermal energy availability. The total daily water

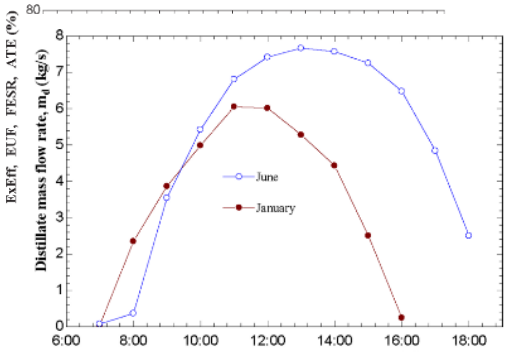

Figure 9
Figure 11

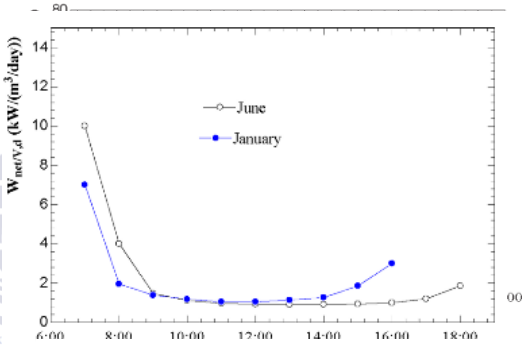

Figure 10
Figure 12

production is substantially greater in June due to prolonged and more intense solar irradiation.

The power to water ratio demonstrates comparable daily trends for both seasons. The profile is characterized by a sharp decline during morning hours, stabilizes to a relatively constant value near midday, and increases again during the afternoon. This pattern reflects the differential response times between power generation and thermal desalination processes to varying solar input.

4. Conclusion

This study developed and performed a comprehensive thermodynamic analysis of a solar-driven poly-generation system utilizing parabolic trough collectors. The integrated system combined an organic Rankine cycle (ORC) for power generation, a multiple-effect distillation (MED) unit for freshwater production, and an absorption cooling cycle for refrigeration.

The performance of the poly-generation plant was evaluated under the climatic conditions of Lahore, Pakistan, across a range of operating parameters. System performance was quantified using both energy-based and exergy-based metrics, specifically the Energy Utilization Factor (EUF), Artificial Thermal Efficiency (ATE), Fuel Energy Saving Ratio (FESR), and Exergy Efficiency (ExEff). The analysis revealed that while the EUF, ATE, and FESR followed a temporal trend similar to the direct normal irradiance, peaking at solar noon, their absolute values showed significant dispersion. This indicates that the assessment of a poly-generation system's performance is highly dependent on the selected evaluation criterion, and different indicators can lead

to varying interpretations. A key finding was the close numerical agreement between the exergy efficiency and the fuel energy saving factor, suggesting a consistent thermodynamic advantage of the poly-generation system over conventional separate production methods. Furthermore, the fresh water production rate and the power-to-water ratio were calculated for representative seasonal days, providing insight into the system's operational characteristics.

For a more comprehensive and practical assessment of such systems, future work should incorporate additional dimensions of analysis, including detailed economic evaluation (e.g., levelized cost of outputs), environmental impact assessment (e.g., life cycle analysis), and a broader sustainability evaluation to determine the system's viability and potential for implementation.

References

[1] Q. Wang, M. Su, R. Li, and P. Ponce, "The effects of energy prices, urbanization and economic growth on energy consumption per capita in 186 countries," Journal of Cleaner Production, vol. 225, pp. 1017–1032, July 2019, doi: 10.1016/j.jclepro.2019.04.008

[2] T. Bakirtas and A. G. Akpolat, "The relationship between energy consumption, urbanization, and economic growth in new emerging-market countries," Energy, vol. 147, pp. 110–121, Mar. 2018, doi: 10.1016/j.energy.2018.01.011.

[3] A. Lejeune and S. L. Hui, "Hydro Power," Comprehensive Renewable Energy. Elsevier, pp. 15–47, 2012. doi: 10.1016/b978-0-08-087872-0.00602-8.

[4] L. Pang, L. Liu, X. Zhou, M. Hafeez, S. Ullah, and M. T. Sohail, "How does natural resource depletion affect energy security risk? New insights from major energy-consuming countries," Energy Strategy Reviews, vol. 54, p. 101460, July 2024, doi: 10.1016/j.esr.2024.101460.

[5] M. Arzaghi and J. Squalli, "The environmental impact of fossil fuel subsidy policies," Energy Economics, vol. 126, p. 106980, Oct. 2023, doi: 10.1016/j.eneco.2023.106980.

[6] S. E. Hosseini, "Fossil fuel crisis and global warming," Fundamentals of Low Emission Flameless Combustion and Its Applications. Elsevier, pp. 1–11, 2022. doi: 10.1016/b978-0-323-85244-9.00001-0.

[7] Ch. M. S. Kumar et al., "Solar energy: A promising renewable source for meeting energy demand in Indian agriculture applications," Sustainable Energy Technologies and Assessments, vol. 55, p. 102905, Feb. 2023, doi: 10.1016/j.seta.2022.102905.

[8] S. Kuşkaya, F. Bilgili, E. Muğaloğlu, K. Khan, M. E. Hoque, and N. Toguç, "The role of solar energy usage in environmental sustainability: Fresh evidence through time-frequency analyses," Renewable Energy, vol. 206, pp. 858–871, Apr. 2023, doi: 10.1016/j.renene.2023.02.063.

[9] A. Kasaeian, E. Bellos, A. Shamaeizadeh, and C. Tzivanidis, "Solar-driven polygeneration systems: Recent progress and outlook," Applied Energy, vol. 264, p. 114764, Apr. 2020, doi: 10.1016/j.apenergy.2020.114764.

[10] L. Gu et al., "A review of solar dish applications: thermal utilization, thermochemistry, polygeneration and multi-energy complementary systems," Applied Energy, vol. 401, p. 126716, Dec. 2025, doi: 10.1016/j.apenergy.2025.126716.

[11] W. Fuqiang, C. Ziming, T. Jianyu, Y. Yuan, S. Yong, and L. Linhua, "Progress in concentrated solar power technology with parabolic trough collector system: A comprehensive review," Renewable and Sustainable Energy Reviews, vol. 79, pp. 1314–1328, Nov. 2017, doi: 10.1016/j.rser.2017.05.174.

[12] A. Kasaeian, S. Tabasi, J. Ghaderian, and H. Yousefi, "A review on parabolic trough/Fresnel based photovoltaic thermal systems," Renewable and Sustainable Energy Reviews, vol. 91, pp. 193–204, Aug. 2018, doi: 10.1016/j.rser.2018.03.114.

[13] M. Amidpour and M. H. Khoshgoftar Manesh, "Modern polygeneration systems," Cogeneration and Polygeneration Systems. Elsevier, pp. 237–286, 2021. doi: 10.1016/b978-0-12-817249-0.00013-6.

[14] M. Temiz and I. Dincer, "Concentrated solar driven thermochemical hydrogen production plant with thermal energy storage and geothermal systems," Energy, vol. 219, p.

119554, Mar. 2021, doi: 10.1016/j.energy.2020.119554.
[15] L. M. Serra, M.-A. Lozano, J. Ramos, A. V. Ensinas, and S. A. Nebra, "Polygeneration and efficient use of natural resources," Energy, vol. 34, no. 5, pp. 575–586, May 2009, doi: 10.1016/j.energy.2008.08.013.
[16] Y. E. Yuksel and M. Ozturk, "Energy and exergy analysis of renewable energy sources-based integrated system for multi-generation application," IJEX, vol. 22, no. 3, p. 250, 2017, doi: 10.1504/ijex.2017.083170.
[17] J. D. Nixon, P. K. Dey, and P. A. Davies, "The feasibility of hybrid solar-biomass power plants in India," Energy, vol. 46, no. 1, pp. 541–554, Oct. 2012, doi: 10.1016/j.energy.2012.07.058.
[18] R. Loni, A. Kasaeian, O. Mahian, A. Z. Sahin, and S. Wongwises, "Exergy analysis of a solar organic Rankine cycle with square prismatic cavity receiver," IJEX, vol. 22, no. 2, p. 103, 2017, doi: 10.1504/ijex.2017.083011.
[19] A. Atiz, H. Karakilcik, M. Erden, and M. Karakilcik, "Investigation energy, exergy and electricity production performance of an integrated system based on a low-temperature geothermal resource and solar energy," Energy Conversion and Management, vol. 195, pp. 798–809, Sept. 2019, doi: 10.1016/j.enconman.2019.05.056.
[20] E. Akrami, A. Chitsaz, P. Ghamari, and S. M. S. Mahmoudi, "Energy and exergy evaluation of a tri-generation system driven by the geothermal energy," J Mech Sci Technol, vol. 31, no. 1, pp. 401–408, Jan. 2017, doi: 10.1007/s12206-016-1242-y.
[21] D. Maraver, J. Uche, and J. Royo, "Assessment of high temperature organic Rankine cycle engine for polygeneration with MED desalination: A preliminary approach," Energy Conversion and Management, vol. 53, no. 1, pp. 108–117, Jan. 2012, doi: 10.1016/j.enconman.2011.08.013.
[22] R. Mathkor, B. Agnew, M. Al-Weshahi, and F. Latrsh, "Exergetic Analysis of an Integrated Tri-Generation Organic Rankine Cycle," Energies, vol. 8, no. 8, pp. 8835–8856, Aug. 2015, doi: 10.3390/en8088835.
[23] M. F. Ezzat and I. Dincer, "Energy and exergy analyses of a new geothermal–solar energy based system," Solar Energy, vol. 134, pp. 95–106, Sept. 2016, doi: 10.1016/j.solener.2016.04.029.
[24] E. A. Chadegani, M. Sharifishourabi, and F. Hajiarab, "Comprehensive assessment of a multi-generation system integrated with a desalination system: Modeling and analysing," Energy Conversion and Management, vol. 174, pp. 20–32, Oct. 2018, doi: 10.1016/j.enconman.2018.08.011.
[25] S. Ozlu and I. Dincer, "Performance assessment of a new solar energy-based multigeneration system," Energy, vol. 112, pp. 164–178, Oct. 2016, doi: 10.1016/j.energy.2016.06.040.
[26] F. A. Al-Sulaiman, I. Dincer, and F. Hamdullahpur, "Exergy modeling of a new solar driven trigeneration system," Solar Energy, vol. 85, no. 9, pp. 2228–2243, Sept. 2011, doi: 10.1016/j.solener.2011.06.009.
[27] S. Ozlu and I. Dincer, "Analysis and evaluation of a new solar energy-based multigeneration system," Int. J. Energy Res., vol. 40, no. 10, pp. 1339–1354, Mar. 2016, doi: 10.1002/er.3516.
[28] E. Bellos and C. Tzivanidis, "Parametric analysis and optimization of a solar driven trigeneration system based on ORC and absorption heat pump," Journal of Cleaner Production, vol. 161, pp. 493–509, Sept. 2017, doi: 10.1016/j.jclepro.2017.05.159.
[29] S. Li, J. Sui, H. Jin, and J. Zheng, "Full chain energy performance for a combined cooling, heating and power system running with methanol and solar energy," Applied Energy, vol. 112, pp. 673–681, Dec. 2013, doi: 10.1016/j.apenergy.2012.11.018.
[30] B. Eisavi, S. Khalilarya, A. Chitsaz, and M. A. Rosen, "Thermodynamic analysis of a novel combined cooling, heating and power system driven by solar energy," Applied Thermal Engineering, vol. 129, pp. 1219–1229, Jan. 2018, doi: 10.1016/j.applthermaleng.2017.10.132.
[31] R. S. El-Emam and I. Dincer, "Investigation and assessment of a novel solar-driven integrated energy system," Energy Conversion and Management, vol. 158, pp. 246–255, Feb. 2018, doi: 10.1016/j.enconman.2017.12.062.
[32] F. Suleman, I. Dincer, and M. Agelin-Chaab, "Development of an integrated renewable energy

system for multigeneration," Energy, vol. 78, pp. 196–204, Dec. 2014, doi: 10.1016/j.energy.2014.09.082.

[33] C. Yang, X. Wang, M. Huang, S. Ding, and X. Ma, "Design and simulation of gas turbine-based CCHP combined with solar and compressed air energy storage in a hotel building," Energy and Buildings, vol. 153, pp. 412–420, Oct. 2017, doi: 10.1016/j.enbuild.2017.08.035.

[34] S. Islam, I. Dincer, and B. S. Yilbas, "Development, analysis and assessment of solar energy-based multigeneration system with thermoelectric generator," Energy Conversion and Management, vol. 156, pp. 746–756, Jan. 2018, doi: 10.1016/j.enconman.2017.09.039.

[35] F. Khalid, I. Dincer, and M. A. Rosen, "Techno-economic assessment of a renewable energy based integrated multigeneration system for green buildings," Applied Thermal Engineering, vol. 99, pp. 1286–1294, Apr. 2016, doi: 10.1016/j.applthermaleng.2016.01.055.

[36] F. Calise, M. D. d'Accadia, A. Macaluso, A. Piacentino, and L. Vanoli, "Exergetic and exergoeconomic analysis of a novel hybrid solar–geothermal polygeneration system producing energy and water," Energy Conversion and Management, vol. 115, pp. 200–220, May 2016, doi: 10.1016/j.enconman.2016.02.029.

[37] M. Almahdi, I. Dincer, and M. A. Rosen, "A new solar based multigeneration system with hot and cold thermal storages and hydrogen production," Renewable Energy, vol. 91, pp. 302–314, June 2016, doi: 10.1016/j.renene.2016.01.069.

[38] Y. E. Yuksel, M. Ozturk, and I. Dincer, "Thermodynamic performance assessment of a novel environmentally-benign solar energy based integrated system," Energy Conversion and Management, vol. 119, pp. 109–120, July 2016, doi: 10.1016/j.enconman.2016.04.040.

[39] E. Bellos, L. Vellios, I.-C. Theodosiou, and C. Tzivanidis, "Investigation of a solar-biomass polygeneration system," Energy Conversion and Management, vol. 173, pp. 283–295, Oct. 2018, doi: 10.1016/j.enconman.2018.07.093.

[40] S. Karellas and K. Braimakis, "Energy–exergy analysis and economic investigation of a cogeneration and trigeneration ORC–VCC hybrid system utilizing biomass fuel and solar power," Energy Conversion and Management, vol. 107, pp. 103–113, Jan. 2016, doi: 10.1016/j.enconman.2015.06.080.

[41] M. Al-Ali and I. Dincer, "Energetic and exergetic studies of a multigenerational solar–geothermal system," Applied Thermal Engineering, vol. 71, no. 1, pp. 16–23, Oct. 2014, doi: 10.1016/j.applthermaleng.2014.06.033.

[42] A. M. Pantaleo, S. M. Camporeale, A. Miliozzi, V. Russo, N. Shah, and C. N. Markides, "Novel hybrid CSP-biomass CHP for flexible generation: Thermo-economic analysis and profitability assessment," Applied Energy, vol. 204, pp. 994–1006, Oct. 2017, doi: 10.1016/j.apenergy.2017.05.019.

[43] Q. Wu, H. Ren, W. Gao, P. Weng, and J. Ren, "Design and operation optimization of organic Rankine cycle coupled trigeneration systems," Energy, vol. 142, pp. 666–677, Jan. 2018, doi: 10.1016/j.energy.2017.10.075.

[44] Y. N. Dabwan, P. Gang, J. Li, G. Gao, and J. Feng, "Development and assessment of integrating parabolic trough collectors with gas turbine trigeneration system for producing electricity, chilled water, and freshwater," Energy, vol. 162, pp. 364–379, Nov. 2018, doi: 10.1016/j.energy.2018.07.211.

[45] F. Khalid, I. Dincer, and M. A. Rosen, "Thermoeconomic analysis of a solar-biomass integrated multigeneration system for a community," Applied Thermal Engineering, vol. 120, pp. 645–653, June 2017, doi: 10.1016/j.applthermaleng.2017.03.040.

[46] S. Li, J. Sui, H. Jin, and J. Zheng, "Full chain energy performance for a combined cooling, heating and power system running with methanol and solar energy," Applied Energy, vol. 112, pp. 673–681, Dec. 2013, doi: 10.1016/j.apenergy.2012.11.018.

[47] H. Li, X. Zhang, L. Liu, R. Zeng, and G. Zhang, "Exergy and environmental assessments of a novel trigeneration system taking biomass and solar energy as co-feeds," Applied Thermal Engineering, vol. 104, pp. 697–706, July 2016, doi: 10.1016/j.applthermaleng.2016.05.081.

[48] F. Calise, "Design of a hybrid polygeneration system with solar collectors and a Solid Oxide

Fuel Cell: Dynamic simulation and economic assessment," International Journal of Hydrogen Energy, vol. 36, no. 10, pp. 6128–6150, May 2011, doi: 10.1016/j.ijhydene.2011.02.057.

[49] J. Wang, J. Wu, Z. Xu, and M. Li, "Thermodynamic performance analysis of a fuel cell trigeneration system integrated with solar-assisted methanol reforming," Energy Conversion and Management, vol. 150, pp. 81–89, Oct. 2017, doi: 10.1016/j.enconman.2017.08.012.

[50] E. Bellos and C. Tzivanidis, "Multi-objective optimization of a solar driven trigeneration system," Energy, vol. 149, pp. 47–62, Apr. 2018, doi: 10.1016/j.energy.2018.02.054.

[51] B. Eisavi, S. Khalilarya, A. Chitsaz, and M. A. Rosen, "Thermodynamic analysis of a novel combined cooling, heating and power system driven by solar energy," Applied Thermal Engineering, vol. 129, pp. 1219–1229, Jan. 2018, doi: 10.1016/j.applthermaleng.2017.10.132.

[52] U. Çakir, K. Çomakli, and F. Yüksel, "The role of cogeneration systems in sustainability of energy," Energy Conversion and Management, vol. 63, pp. 196–202, Nov. 2012, doi: 10.1016/j.enconman.2012.01.041.

[53] M. Kanoglu, I. Dincer, and M. A. Rosen, "Understanding energy and exergy efficiencies for improved energy management in power plants," Energy Policy, vol. 35, no. 7, pp. 3967–3978, July 2007, doi: 10.1016/j.enpol.2007.01.015.

[54] I. Dincer and H. Al-Muslim, "Thermodynamic analysis of reheat cycle steam power plants," Int. J. Energy Res., vol. 25, no. 8, pp. 727–739, 2001, doi: 10.1002/er.717.

[55] E. Minciuc, O. Le Corre, V. Athanasovici, M. Tazerout, and I. Bitir, "Thermodynamic analysis of tri-generation with absorption chilling machine," Applied Thermal Engineering, vol. 23, no. 11, pp. 1391–1405, Aug. 2003, doi: 10.1016/s1359-4311(03)00067-x.

[56] P. Ahmadi, I. Dincer, and M. A. Rosen, "Exergo-environmental analysis of an integrated organic Rankine cycle for trigeneration," Energy Conversion and Management, vol. 64, pp. 447–453, Dec. 2012, doi: 10.1016/j.enconman.2012.06.001.

[57] M. Ameri, A. Behbahaninia, and A. A. Tanha, "Thermodynamic analysis of a tri-generation system based on micro-gas turbine with a steam ejector refrigeration system," Energy, vol. 35, no. 5, pp. 2203–2209, May 2010, doi: 10.1016/j.energy.2010.02.006.

[58] E. Cardona and A. Piacentino, "A methodology for sizing a trigeneration plant in mediterranean areas," Applied Thermal Engineering, vol. 23, no. 13, pp. 1665–1680, Sept. 2003, doi: 10.1016/s1359-4311(03)00130-3.

[59] A. M. El-Nashar, "Cogeneration for power and desalination — state of the art review," Desalination, vol. 134, no. 1–3, pp. 7–28, Apr. 2001, doi: 10.1016/s0011-9164(01)00111-4.

[60] B. F. Tchanche, G. Papadakis, G. Lambrinos, and A. Frangoudakis, "Fluid selection for a low-temperature solar organic Rankine cycle," Applied Thermal Engineering, vol. 29, no. 11–12, pp. 2468–2476, Aug. 2009, doi: 10.1016/j.applthermaleng.2008.12.025.

[61] G. Pei, J. Li, and J. Ji, "Analysis of low temperature solar thermal electric generation using regenerative Organic Rankine Cycle," Applied Thermal Engineering, vol. 30, no. 8–9, pp. 998–1004, June 2010, doi: 10.1016/j.applthermaleng.2010.01.011.

[62] www.Skyfuel.com "Sky Trough @Fact sheet 2011".

[63] Therminol. Heat transfer fluids by Solutia Inc., Therminol VP-1. www.therminol.com/pages/products/vp-1.asp; Aug. 2012.

[64] M. J. Montes, A. Abánades, and J. M. Martínez-Val, "Performance of a direct steam generation solar thermal power plant for electricity production as a function of the solar multiple," Solar Energy, vol. 83, no. 5, pp. 679–689, May 2009, doi: 10.1016/j.solener.2008.10.015.

[65] S.A. Klein, Engineering equation solver (EES), Academic com mercial Version 9.725, F-chart; 2014. http://www.fchart.com/ ees/.

[66] S. A. Kalogirou, "Solar thermal collectors and applications," Progress in Energy and Combustion Science, vol. 30, no. 3, pp. 231–295, 2004, doi: 10.1016/j.pecs.2004.02.001.

[67] S. T. Mohammad, H. H. Al-Kayiem, M. K. Assadi, Osama. Sabir, and A. K. Khlief, "An integrated program of a stand-alone parabolic trough solar thermal power plant: Code description and test," Case Studies in Thermal Engineering, vol. 12, pp. 26–37, Sept. 2018, doi: 10.1016/j.csite.2018.02.006.

[68] H. El-Dessouky, I. Alatiqi, S. Bingulac, and H. Ettouney, "Steady-State Analysis of the Multiple Effect Evaporation Desalination Process," Chem. Eng. Technol., vol. 21, no. 5, p. 437, May 1998, doi: 10.1002/(sici)1521-4125(199805)21:5<437::aid-ceat437>3.0.co;2-d.

[69] K. H. Mistry, M. A. Antar, and J. H. Lienhard V, "An improved model for multiple effect distillation," Desalination and Water Treatment, vol. 51, no. 4–6, pp. 807–821, Jan. 2013, doi: 10.1080/19443994.2012.703383.

[70] R. K. Kamali, A. Abbassi, S. A. Sadough Vanini, and M. Saffar Avval, "Thermodynamic design and parametric study of MED-TVC," Desalination, vol. 222, no. 1–3, pp. 596–604, Mar. 2008, doi: 10.1016/j.desal.2007.01.120.

[71] D. Zhao, J. Xue, S. Li, H. Sun, and Q. Zhang, "Theoretical analyses of thermal and economical aspects of multi-effect distillation desalination dealing with high-salinity wastewater," Desalination, vol. 273, no. 2–3, pp. 292–298, June 2011, doi: 10.1016/j.desal.2011.01.048.

[72] C. Kutscher, F. Burkholder, K. Stynes, Generation of Parabolic Trough Collector Efficiency curve from Separate measure ments of outdoor optical efficiency and indoor receiver heat loss, National Renewable Energy Laboratory Presented at Solar PACES 2010 Perpignan, France, p. 7.

[73] H. D. Madhawa Hettiarachchi, M. Golubovic, W. M. Worek, and Y. Ikegami, "Optimum design criteria for an Organic Rankine cycle using low-temperature geothermal heat sources," Energy, vol. 32, no. 9, pp. 1698–1706, Sept. 2007, doi: 10.1016/j.energy.2007.01.005.

[74] M. Balghouthi, M. H. Chahbani, and A. Guizani, "Feasibility of solar absorption air conditioning in Tunisia," Building and Environment, vol. 43, no. 9, pp. 1459–1470, Sept. 2008, doi: 10.1016/j.buildenv.2007.08.003.